Modeling of Low-Energy Neutron Scattering in Liquid Hydrogen Using NCrystal

LUND
UNIVERSITY

This Master Thesis has been carried out by Tim Günter at the
European Spallation Source (ESS)
and the Lund University Department of Physics, Division of Nuclear Physics
under the supervision of
Dr. Douglas DiJulio, Dr. Jose Ignacio Marquez Damian, Prof. Joakim Cederkäll
Duration: 4 months, Examination: June 2022

Abstract

The European Spallation Source ESS, under construction in Lund, Sweden, aims to produce high-brightness and intensity neutrons for a multitude of experiments upon completion. An efficient production of neutrons requires elaborate understanding of the moderation process which slows the neutrons from relativistic speed to a kinetic energy of meV. The moderator used at the ESS will be partially made of water and liquid para-hydrogen, which enables simultaneous production of thermal and cold neutrons. The interaction between neutrons and the moderator is best described by the total neutron scattering cross section which in turn is computationally derived from the scattering kernel. The liquid hydrogen kernel itself includes models of a self- and distinct scattering function which describe the interaction of individual molecules with neutrons as well as interference effects of scattered matter waves from neighboring molecules.

Scattering kernels are commonly produced by a software called NJOY, however, an effort at ESS has been made to develop and transition to a new software called NCrystal. Its more flexible design allows for easier implementation of physics models beyond what is currently included in NJOY for more moderator materials. Thus far, NCrystal is primarily aimed at generating scattering kernels for poly-crystalline materials in solid phase, a capability which was now expanded to liquid water and liquid hydrogen. The resulting cross sections were bench-marked against proven software and show good agreement.

Acknowledgements

I would like to thank my supervisor Douglas Di Julio for his great help during the project and for sharing his valuable knowledge with me! I would like to thank Ignacio Damian Marquez for being a great supervisor and providing valuable input to the project! I want to thank my university supervisor Joakim Cederkäll for providing me the opportunity of working on such an interesting project! I would also like to thank the ESS spallation physics group for welcoming me into the team and creating a productive and enjoyable work place!

I want to thank the ESS for providing me with generous funding for completing this project.

Lastly, I want to thank my parents, my brother and my grandparents for their support and my friends for cheering me up in stressful times.

Contents

List of Figures

1 Introduction

1.1 ESS

The European Spallation Source (ESS) is a neutron source currently under construction in Lund, Sweden. Upon completion, it will be the most luminous neutron source world wide with the aim to provide a time average power of 5 MW with a peak power of 125 MW [1]. ESS will be the first long pulse spallation facility, with a beam pulse duration of 2.86 ms at a 14 Hz repetition rate. For neutron production, the facility will use the phenomenon of *spallation*, where a linear accelerator produces a proton beam of an aspirational energy of 2 GeV, which impacts on a rotating tungsten target wheel. Tungsten is chosen as the target material because it has a very neutron rich nucleus but is still stable. The protons, which are traveling at 90 % of the speed of light, are energetic enough to tear apart the nuclei of the target and in the process release several, still very energetic neutrons [2]. While the proton beam characteristics are important quantities to describe the performance of the facility, the determining measure for many of the planned experiments is the brightness in both, *cold* and *thermal neutrons*. These terms describe energy ranges of the neutrons which are finally delivered to the experiments. Thermal neutrons have an energy of around 25 meV and are in a thermal equilibrium with a room temperature moderator, typically water. Cold neutrons on the other hand can only be generated with the use of a cryogenic moderator, in case of ESS liquid para-hydrogen. To achieve an effective production of neutrons in the range of a few meV, generated from the initial neutrons in the MeV range, an efficient moderator is required [3].

1.2 The ESS moderator

The design goals of the facility are to enable studies with both, cold and thermal neutrons in many different instruments [1]. This constrains the design of the moderator to allow for a geometrically dependent extraction of neutrons of differing energies. The final design is that of the *butterfly moderator*, which consists of an outer shell filled with light water and a core with liquid para-hydrogen, contained by an aluminium casing [1], see fig. 1.

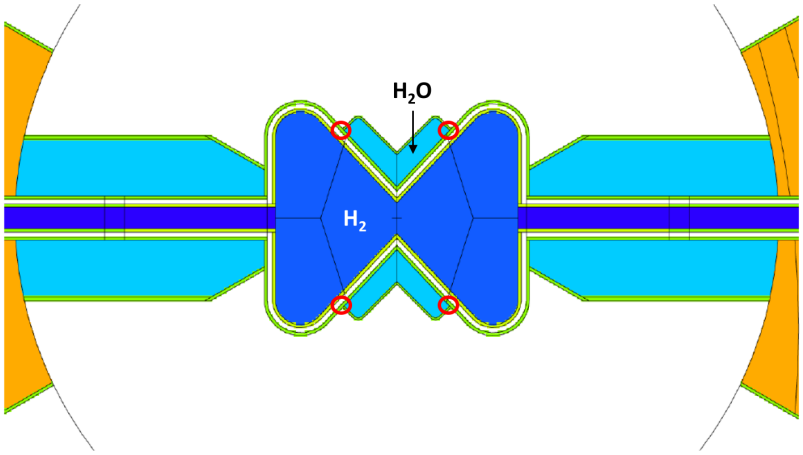

Figure 1: The ESS butterfly moderator consisting of water and liquid hydrogen [4]. Neutrons enter the moderator into the image plane and exit to the top and bottom after scattering. Thermal neutrons are concentrated towards the center, cold neutrons further to the edges.

Since the neutrons will always enter the the moderator from the same side, Monte-Carlo simulations could be used to determine the neutrons spectra at different outflow channels of the moderator. The described configuration yields a thermal spectrum closer to center of the beam axis of the moderator while the spectrum is colder closer to the edges [4]. It is worth noting that there are no regions where there are neutrons exclusively of one energy, rather there is always a relatively wide distribution. Experiments have to be designed to work with such a spectrum. However, there are spatial concentrations of different neutron energies as described above.

1.3 Objective of the thesis

The calculation of thermal and sub-thermal neutron sources using Monte-Carlo radiation transport codes mainly relies on the usage of the thermal scattering library produced with the NJOY code [5]. The library is based on the microscopic condensed matter properties of the material and computed using nuclear data evaluation tools. The computational architecture of the library limits its use for modern Monte-Carlo applications and hinders implementation of new physics models. Thus, there have been efforts to develop a new thermal scattering library generation software based on a software called NCrystal [6] with a modern and flexible design, which could eventually be an alternative to NJOY. It is written in `C++` but also includes modules to link it with Python scripts which makes it easier to add new functionalities. Currently, NCrystal primarily supports calculations of scattering kernels for solid poly-crystalline materials [6]. This Master thesis aims to expand the functionality of NCrystal to allow the calculation of scattering kernels of some simple gases and liquids with the main interest being directed to liquid para-hydrogen, which will be used as part of the moderator at

ESS. The physics models needed to represent this material include a translational part which is based on a diffusion model to account for the movement of the molecules in a liquid [7]. Rotational and vibrational modes as well as spin-correlation between the atoms are the inner-molecular effects to be considered [8]. Since the moderator will be very cold at $T \approx 20$ K, interference effects have to be accounted for as well by the means of coherent scattering [9]. This work presents an overview of the implementation of these models to the existing NCrystal architecture.

1.4 History of thermal scattering law of hydrogen

Young and Koppel (YK) [8] published their theoretical evaluation of a hydrogen scattering cross section in 1964 already with the intention of cold neutron production for neutron scattering experiments and not primarily for application in nuclear power reactors. The model delivers a description of the neutron scattering cross section for hydrogen gas from 0-3 eV neutron energy and gas temperature $T \leq 3000$ K. It is also applicable for liquid hydrogen for neutron energies greater than 0.007 eV. The model includes spin correlation between the atoms as well as molecular rotation and vibration, however, it does not consider rotation-vibration coupling. Rotations are calculated under the assumptions that the hydrogen molecule is of a dumbbell shape and rotates around its center of mass. The translational component is assumed to be that of a free gas, which means there are no interactions between molecules at high temperatures. Consequently, this means that the model has limitations at low temperatures in the liquid phase.

After numerous neutron scattering experiments had shown that YK's assumptions were too simplifying in some instances (mainly Seiffert et al. in 1970 [10]), Utsuro published a revised model in 1977 [11]. The main goal was to improve the accuracy at energies between 0.1 meV and 0.3 eV, i.e. in the range of slow neutrons. Generally, the translation of the molecules cannot be well described with a free gas model and Utsuro thus reverts to using a superposition of a solid-like movement and a diffusion model. To arrive at a more concise expression for the final cross section, the reasonable assumption is made that, at the given energies, the molecule always remains in the lowest vibrational state. This allows to neglect the rather complicated description of vibrations.

Following this, Keinert and Sax [7] further improved on the translational contribution in their paper from 1987. Instead of the solid-diffusion model from Utsuro [11], they choose a model with a slightly modified solid part and a hindered translation model instead of the diffusion model. For the first time the quantity of the *scattering kernel* $S(\alpha, \beta)$ in terms of the dimensionless momentum transfer α and the dimensionless energy transfer β instead of differential cross sections are used. The improved kernel is calculated as a convolution of the modified YK model (without vibrations) and the

just described translational part. This approach was also adopted in NJOY [5], the standard code used for scattering library generation until now. Furthermore, at low energy, interference between neutron matter waves (coherent scattering) is implemented into NJOY with the Vineyard approximation, which is not originally part of the Keinert and Sax model.

In the following years, experimental work went into understating the translational processes in condensed matter, which subsequently motivated the work of Granada et al. [12][13]. They introduced an updated phonon frequency spectrum based on new theoretical considerations. After previous models had usually neglected intramolecular vibrations, this work also presented an approach to model vibrations by using a separate frequency distribution essentially consisting of δ-functions at the energies of the vibrational transitions. This is a different description compared to Young and Koppel in the original model, who described vibrations as quantum mechanical properties of the molecules in an operator description (see section 2.3.3 for a mathematical derivation). These two spectra are convoluted, followed by a second convolution also considering a diffusion term like it was already the case in the Keinert and Sax model. While these changes mainly improve the accuracy at higher neutron energy, Granada et al. also corrected an error in the vineyard approximation of the NJOY implementation of the Keinert and Sax model.

After the revised model was introduced, it took several years until new cross section measurements were carried out. In 2015 Grammer et al. [14] published their findings from a new experiment, measuring the total cross section of para-hydrogen to be differing by a factor of 3 from the experiments of Seiffert et al. [10] at an energy of 1 meV. The authors theorize that the difference comes down to an undetected contamination with ortho-hydrogen in the previous experiment. To support this, a model is presented where a combination of their results with an additional assumed 5% ortho-hydrogen proportion matches the previous result of Seiffert et al., suggesting their sample was indeed contaminated.

These findings reinvigorated interest into theoretical and computational models of neutron scattering in molecular hydrogens. Guarini et al. [15] show consequently that the *distinct* part of the scattering function is responsible for the deviations by doing Path integral molecular dynamics (PIMD) [16] calculations. This is down to interference effects, also called coherent scattering, which become one of the dominant mechanisms in neutron interaction in hydrogens at low energy and will later be referred to as *distinct* part of the scattering kernel. These calculations match the total cross sections found by Grammer et al. very well. A scattering kernel itself was, however, not calculated in this work. This was done by Marquez Damian et al. [17], where data based on experimental results was used as input for the scattering kernel. To account for the distinct dynamics the so-called Sköld approximation [18] for coherent scattering was used to finally obtain a new scattering kernel which can replicate the total cross

section found by Grammer.

The two above mentioned methods were later combined by Marquez Damian, DiJulio and Muhrer [19] as well as two Master theses [20][21] at the ESS such that PIMD calculations were used directly to create the scattering kernels. This allowed for temperature dependent effects in the input data to be accounted for. The molecular dynamics approach and the Sköld approximation were put together into a modified version of the NJOY neutron scattering library to calculate a kernel which accurately reproduces the experimental data. This thesis aims to implement this model into a newer scattering library called NCrystal.

2 Thermal Neutron Scattering

2.1 Overview

For neutron scattering experiments it is essential that the neutrons have a sufficiently small kinetic energy. From their creation in the target to the experiment their energy has to reduced by around nine orders of magnitude (from MeV to meV). This process happens in the moderator and is described by thermal neutron scattering, and also referred to as *slowing down* and *thermalization* [3]. In general, the moderation process must be separated into two regions of differing energies. Firstly, for neutron energies higher than 1 eV the nuclei of the moderator can be treated to be at rest, so everything can be calculated in the laboratory frame without problems. Furthermore, the neutron energy is higher than the binding energy of moderator molecules, thus they can be considered to be unbound and no intermolecular effects have to be considered. In this energy region, almost every neutron-nucleus interaction can be considered as *down-scattering*, i.e. the neutron loses energy, hence this region called *slowing-down region*. When the neutron reaches an energy comparable to the temperature of the moderator it can no longer be slowed down. The neutron is then in equilibrium with the moderator and considered to be thermalized [3]. At this point, the neutrons may be used for some experiments, however, there will be experiments at ESS which require colder neutrons and thus a colder moderator, which in this case will be liquid para-hydrogen.

When the neutron reaches energies lower than approximately 1 eV, many of these simplifications are not valid anymore and a more sophisticated model has to be built. For instance, the scattering nuclei have a comparable kinetic energy to the neutrons and thus they can no longer be treated to be at rest. All calculations can then simplified in a center-of-mass reference frame. Furthermore, neutrons may now gain as well as lose energy during collision, i.e. *upscattering* is allowed. Additionally, molecular or lattice-effects have to be considered since the interactions are now more subtle and the energy scales of for example rotational or diffusion effects coincide with the neutron energy. In case of solid moderators, the nucleus's recoil will be translated into lattice vibrations [3], which in solid state physics are called phonons. Phonon-neutron interactions play a fundamental role in the description of solid and even liquid moderators, as will be shown later. The third effect which has to be considered for lower energies is that of *coherent scattering*. A lower neutron energy means that the deBroglie-wavelength of the particles will be of the same order of magnitude as intermolecular distances in a liquid or the lattice constant in a solid. Hence, there are interference effects to be considered which can depend on many factors like the angle of incidence on a solid or, most importantly, the neutron energy [3]. The three effects described now will be illustrated with mathematical derivations in the following chapters.

2.2 Thermal Scattering Law

The quantity that describes the interaction of a neutron with the moderator is the double differential cross section $\frac{d^2\sigma}{d\Omega d\omega}$ where Ω is the solid angle of the outgoing neutron and ω is the change in energy of the neutron [22]. However, the commonly used thermal scattering libraries usually use a function S, called *thermal scattering law* (TSL) or *scattering kernel*. Their relation is given by [22]

$$\frac{d^2\sigma}{d\Omega d\omega} = \frac{\sigma_b}{2}\sqrt{\frac{E'}{E}}S(Q,\omega) \tag{1}$$

with the momentum transfer Q and the energy transfer ω, i.e. ω is the frequency of the photon corresponding to the energy transfer: $\omega = \frac{E'-E}{\hbar}$ where $\hbar$ is the reduced Planck constant, E' and E the initial and final neutron energy. In the literature, the *scattering kernel* is often written in terms of the dimensionless momentum transfer α and the dimensionless energy transfer β:

$$\alpha = \frac{E' + E - 2\sqrt{EE'}\cos\theta}{M/m_n k_B T}\,;\ \beta = \frac{E'-E}{k_B T}\,. \tag{2}$$

Here σ_b is the bound scattering cross section of the atom, T the temperature of the moderator, M the mass of the molecule, m_n the mass of the neutron, θ the scattering angle and k_B Boltzmann's constant. The two different notations of the scattering kernel are related by

$$S(\alpha,\beta) = \frac{k_B T}{\hbar}S(Q,\omega)\,. \tag{3}$$

The parameters α, β, Q and ω can also be related by the expressions [22]:

$$\alpha = \frac{\hbar^2 Q^2}{2Mk_B T}\,,\ \beta = \frac{\hbar\omega}{k_B T}\,. \tag{4}$$

2.3 Neutron scattering in molecular hydrogen

The goal of the thesis is to implement a physics model for calculating a scattering kernel for liquid para-hydrogen, the cold moderator of ESS. A hydrogen atom has a nuclear spin of $s = \frac{1}{2}$ which results in two possible spin configurations for a diatomic hydrogen molecule. They are called para-hydrogen in the case of an anti-parallel total spin alignment $S = 0$ and ortho-hydrogen for parallel alignment with $S = 1$ [8].

When an incoming neutron scatters off a hydrogen molecule, the spin interaction of the two atoms has an effect on the energy and momentum transfer and thus on the double differential cross section. Further innermolecular effects to be considered is the rotation of the molecule around its center of mass as well as possible vibrations. In addition one has to consider the motion of the molecule itself which may be described in a variety of models. In combination with a coherent scattering contribution to the

TSL, one can generally write [9]

$$\frac{d^2\sigma}{d\Omega d\omega} = \frac{1}{2\pi}\frac{k}{k_0}\left(u(Q)\, S_{d,cm}(Q,\omega) + \sum_{J_0 J_1 n_1 l} F(Q, J_0, J_1, n_1, l)\, S_{s,cm}(Q, \omega - \omega_{J_0 J_1} - \omega_{n_0 n_1})\right), \tag{5}$$

where $S_{d,cm}$ is the *distinct* scattering function, which refers to the coherent scattering part. The index *cm* marks that the scattering kernel is calculated in the center-of-mass reference frame of the molecule. The other term $S_{s,cm}$ calculates the incoherent scattering which can be added to the coherent part to obtain the full cross secction. It consists of the *self* part which, as will later be shown, is the translational part made up of a solid-type contribution and a diffusion model. The function F encompasses all intramolecular mechanisms as briefly touched upon before and later discussed in greater detail. The entire second term is called S_{cm} and referred to as total dynamic structure factor or total self part. For generality, this equation also includes vibrational effects, marked by the quantum numbers n, which at cold temperatures can later be neglected. $u(Q)$ is a weight function which is dependent on the bound scattering cross section of the atom σ_b which in turn is given by the coherent and incoherent scattering lengths a_c and a_i [9]

$$\sigma_b = 4\pi\left(a_c^2 + a_i^2\right). \tag{6}$$

2.3.1 Coherent and incoherent scattering

In quantum mechanics, particles can under certain conditions show effects that are described by electromagnetic wave propagation. Every particle can thus be connected to a corresponding wavelength, the *De Broglie wavelength*, which is dependent on the particles energy. For relativistic particles one thus has to take the rest mass and the kinetic energy E into account and for neutrons specifically, the De Broglie wavelength is [20]:

$$\lambda\,[\text{Å}] = \frac{9.045}{\sqrt{E\,[\text{meV}]}}. \tag{7}$$

Looking for example at the hydrogen molecule, the bond length between the two atoms is 0.74 Å. With eq. (7) one finds that for a kinetic energy below 150 meV the neutron wavelength is comparable to the bond length. For these low energies, neutron waves scattered from neighboring molecules may interfere with each other, or in other words coherent scattering has to be considered to accurately describe the cross section. The cross section can then be divided into a coherent and an incoherent part, which is simply added up, see eq. (5). In that equation, the coherent term is also called the *distinct* term $S_{d,cm}$ and the incoherent contribution is called the *self* term $S_{s,cm}$.

The distinct part describes the interaction of De Broglie waves of different molecules, whereas the self part describes the scattering effects of one molecule itself.

For this project, the coherent part was calculated by using the Sköld approximation [18]

$$S_{d,cm}(Q,\omega) = S(Q) \cdot S_{s,cm}\left(\frac{Q}{\sqrt{S(Q)}},\omega\right), \tag{8}$$

where $S(Q)$ is the *static structure factor* which considers correlation of positions of nearby molecules. Depending on the molecular structure of the medium, scattering events from neighboring molecules may cause effects like interference. $S(Q)$ quantifies how these effects impact the intensity of the neutron beam after it was scattered by the material. The static structure factor can, however, only describe this very specific part of the scattering which is why all the other calculations, described in the following chapters, are necessary. It can be found experimentally but also be calculated by using molecular dynamic simulations, which is how the factor used for this work was obtained. The calculation itself was not part of this work.

2.3.2 Spin-correlation

To more explicitly derive the form of the function F it is useful to first look at the effect of spin correlation on the cross section. A comprehensive derivation was made in the original paper about thermal neutron scattering by Young and Koppel in 1964 [8]. For the coherent part of the cross section, one can write:

$$\begin{aligned}\frac{d^2\sigma}{d\Omega d\omega} = \frac{1}{2\pi}\frac{k}{k_0}\sum_f \int_{-\infty}^{\infty} dt \sum_l \langle\psi_{it}|\exp[-i\boldsymbol{Q}\cdot\boldsymbol{r}_l(0)] \times \exp[i\boldsymbol{Q}\cdot\boldsymbol{r}_l(t)]|\psi_{it}\rangle_T \\ \times \left[|\langle\psi_f|\sum_{n=1}^{2} a_{ln}\exp[(-1)^n i\boldsymbol{Q}\cdot\boldsymbol{R}_l/2]|\psi_i\rangle|^2 \exp[+i(\epsilon - E_i' + E_f')t]\right]_T\end{aligned} \tag{9}$$

This equation separates the translational part by using the initial wave functions of the translational part ψ_{it} as well as the initial and final energies of just the rotational and vibrational part, E_i' and E_f'. $\boldsymbol{r}_l$ is the vector of the center of mass of molecule l. The factor $(-1)^n$ refers to the center-of-mass system, i.e. for $n = 1, 2$ each of the atoms of either side of the center of mass is addressed. This n should not be confused with the later introduced vibrational quantum number n, which should not be too problematic since the n used here will disappear over the next steps in the derivation. It is important to note that the vector for each atom to the molecule's center of mass, $\boldsymbol{R}_l$, is not constant because of the vibro-rotational motion. In this equation l refers to a specific molecule. Later, it will change to note the summation over different angular momentum states. Again, this is not problematic since the cross section will finally be

calculated per molecule anyways and this l will not occur anymore. ω is the neutron energy transfer and $\boldsymbol{Q}$ the neutron momentum transfer. The index T denotes that the initial states must be taken as the thermal average.

This equation must now be filled with appropriate physics models. Firstly, the non-translational second part of eq. (9) shall be called $g(t)$. For para-hydrogen the total angular momentum $J = |L + S|$ must be of even values. $g(t)$ can be rewritten in the form

$$\begin{aligned} g(t) = &\sum_{J,S} \frac{P_{J,S}}{2J+1} \frac{1}{2S+1} \frac{1}{2} \sum_{\sigma_z, \sigma_z' = \pm\frac{1}{2}} \sum_{J'} e^{i(E_{J'} - E_J)t} \\ &\times \sum_{n=0} e^{in\omega t} \sum_{J_z J_z'} \sum_{S'} \sum_{S_z S_z'} |\langle J' J_z', \, S' S_z', \, \sigma_z', \, n | A | J J_z, \, S S_z, \, \sigma_z, \, n = 0 \rangle|^2 \,, \end{aligned} \tag{10}$$

where A is a spin- and rotation dependent operator which contains information about momentum transfer and how that translates into rotation, J, J' are the initial and final angular momentum states of the molecules with J_z, J_z' being their z-components. S, S' are the initial and final total spin of the molecule, S_z, S_z' their z-components. σ_z, σ_z' are the initial and final z-component of the neutron spin and E_J the rotational energy of the state J. $P_{J,S}$ is the statistical weight of state J with spin S and n is the vibrational quantum number. First, para-hydrogen is considered which means that only the symmetrical matrix elements of A contribute. The initial and final states of the molecule are called i and f and after rewriting the operator in more convenient terms with introducing the Hermitian operator P, the sums can be simplified to

$$\sum_{\sigma_z' S' S_z'} |\langle i | A | f \rangle|^2 = |\langle J' J_z' n | \cos(\boldsymbol{Q} \cdot \boldsymbol{R}/2) | J J_z n = 0 \rangle|^2 \times \langle \sigma_z S S_z | P^2 | \sigma_z S S_z \rangle \,. \tag{11}$$

The second term may be simplified to

$$\sum_{\sigma_z} \langle \sigma_z S S_z | P^2 | \sigma_z S S_z \rangle = 8[a_\mathrm{c}^2 + \frac{1}{3} a_\mathrm{i} S(S+1)] \,. \tag{12}$$

The last two equations can now be substituted into eq. (10) to yield, for spin-conserving transitions:

$$\begin{aligned} g_{S=S'}(t) = &4 \sum_{J} \frac{P_{JS}}{2J+1} \left[a_\mathrm{c}^2 + \frac{a_\mathrm{i}^2}{3} S(S+1) \right] \\ &\times {\sum_{J'}}' \exp[i(E_{J'} - E_J)t] \sum_{n=0} e^{in\omega t} \\ &\times \sum_{J_z J_z'} |\langle J' J_z' n | \cos(\boldsymbol{Q} \cdot \boldsymbol{R}/2) | J J_z n = 0 \rangle|^2 \end{aligned} \tag{13}$$

Here $\sum'_{J'}$ sums over all states of same parity as J. For the corresponding expression for states of opposite parity (ortho-hydrogen), a similar calculation can be made which can be found in [8].

2.3.3 Molecular vibrations

To implement the effect of molecular vibrations into the model, the third term of eq. (13) has to be inspected further. For vibrations to have an effect on the neutron cross section, the incident neutron energy must be large enough so that it cannot gain energy from an interaction, i.e. we only look at downscattering in this model. It is furthermore assumed that the vibrational potential of the H-H bond is harmonic and the distance can be described as $R = a+x$, where x is a small perturbation. Expanding x then yields [8]:

$$x = i(M\omega)^{-1/2}[b - b^\dagger]\,, \tag{14}$$

where b and $b^\dagger$ are the boson creation and annihilation operators. This can be used to determine the matrix element of the third term in eq. (13) with μ being the cosine of the scattering angle:

$$\langle n|e^{\pm i\kappa R\mu/2}|0\rangle = e^{\pm\kappa a\mu/2} \times \langle n|\exp\left[\mp(Q\mu/2(M\omega)^{1/2})(b-b^\dagger)\right]|0\rangle\,, \tag{15}$$

and after a few steps of algebra for $g(t)$ one obtains for even spin parity:

$$\begin{aligned} g_{S=S'}(t) = 4\sum_J \frac{P_{JS}}{2J+1}\left[a_\mathrm{c}^2 + \frac{a_\mathrm{i}^2}{3}S(S+1)\right] \\ \times \sum_{J'}{}' \exp[i(E_{J'}-E_J)t]\sum_n e^{in\omega t}\left(\frac{\kappa^2}{4M\omega}\right)^n \frac{1}{n!} \\ \times \sum_{J_z J'_z}\left|\left\langle J'J'_z\left|\mu^n \exp\left(-\frac{\kappa^2\mu^2}{8M\omega}+\frac{i\kappa a\mu}{2}\right)\right|JJ_z\right\rangle\right|^2\,. \end{aligned} \tag{16}$$

This approximation holds for up to a vibrational quantum number of $n = 5$.

2.3.4 Rotations

For the next step, the rotational transitions have to be inspected. If the hydrogen is in liquid state, its kinetic energy is $kT \ll 0.015$ eV and the molecules always remain in the lowest rotational state. For higher energy, the coupling between different rotational states has to be considered. When no vibro-rotational coupling is considered, the wave-functions of the rotational states can be written as spherical harmonics $|JJ_z\rangle = Y_{JJ_z}(\theta,\phi)$. Choosing an appropriate base introduces, with the help of a cou-

pling theorem, the Clebsch-Gordan coefficients $C(l_1 l_2 l; 000)$. For $m_1 = m_2 = 0$ they vanish unless $l_1 + l_2 + l$ is even. Some steps of algebra introduce this new tool into eq. (16) and one obtains:

$$\begin{aligned} g_{S=S'}(t) = &\left[a_{\mathrm{c}}^2 + (a_{\mathrm{i}}^2/3S(S+1)\right] \sum_J P_{JS} \\ &\times \sum_{J'}{}' \exp[i(E_{J'} - E_J)t](2J'+1) \\ &\times \sum_{n=0} e^{in\omega t} \left(\frac{\kappa^2}{4M\omega}\right)^n \frac{1}{n!} \sum_{l=|J'-J|}^{J'+J} |A_{nl}|^2 \cdot C^2(JJ'l;000)\,, \end{aligned} \tag{17}$$

where

$$A_{nl} = \int_{-1}^{1} d\mu\, \mu^n \exp\left(-\frac{Q^2\mu^2}{8M\omega} + \frac{iQa\mu}{2}\right) P_l(\mu)\,, \tag{18}$$

with the Legendre polynomial $P_l(\mu)$ of order l. In her paper [9], Guarini presents a detailed way to arrive from eq. (17) to the general expression for the function F from eq. (5):

$$F(Q, J_0, J_1, n, l) = s_{(J_0 J_1)}\, x_{(J_0)}\, p_{J_0}^{(J_0)}\, \frac{\alpha^{2n}}{4n!}(2J_1+1) \sum_l C^2(J_1 J_0 l; 000)|A_{nl}|^2\,. \tag{19}$$

At the cold temperature of liquid para-hydrogen the molecule is generally contained to the vibrational ground state which symplifies eq. (19) somewhat. The factor $\frac{\alpha^{2n}}{4n!}$ simplifies to 1 since the vibrational quantum number is always $n = 0$. Additionally, for neutron energies below approximately 0.6 eV and no vibrational dependence because of the cold moderator, eq. (18) simplifies to

$$A_{0l} = \int_{-1}^{1} d\mu\, e^{iQa\mu/2} P_l(\mu) = 2i^l j_l\left(\frac{Qa}{2}\right)\,, \tag{20}$$

with the j_l being the spherical Bessel function of order l. $x_{(J_0)}$ is a coefficient which describes the abundance of different species in the moderator itself, species referring to the spin-configurations ortho and para. $p_{J_0}^{(J_0)}$ is the probability that an incoming neutron will either scatter from a para- or ortho-molecule. These two parameters can consequently be set to 1 for this evaluation since we assume that we have a pure para-hydrogen moderator. For this case, one finally has for the s-parameter:

$$s_{ll} = 4a_c^2 + a_i^2\,. \tag{21}$$

The sums here are to be understood as operators, i.e. every sum applies to all the terms that come after it and all the indices are summed over. As a consequence, there

are three levels of summation in this model.

2.3.5 Solid component

The translation, i.e. the self part $S_{s,cm}$ from eq. (5), can be described by a convolution of a solid-type motion and a diffusion- or freegas contribution [5]. NCrystal can currently only calculate the scattering function for polycrystalline materials, i.e. the solid part [6]. When an incident neutron scatters off a molecule in a solid, the lattice transmits a recoil force to its neighbors. This recoil propagation through the crystal can be interpreted as phonons, i.e. quantized lattice vibrations [6]. Although the moderator is in liquid phase, the interaction between neighboring molecules can still be partly described by inelastic scattering in a solid body. Elastic approximations cannot be used since the expansion that is used in that case smooth out features of the crystal vibrations that are important. Sjölander [23] provides a derivation for cold neutron scattering for cubic Bravais lattices, starting with the differential cross section of the Gaussian approximation

$$\frac{d^2\sigma}{d\Omega d\omega} = \frac{A}{2\pi}\frac{k}{k_0}\int_{-\infty}^{\infty} \exp[i(\omega-\omega_0)t]\exp(Q[\gamma(t)-\gamma(0)])\,dt\,, \tag{22}$$

where $\gamma(t)$ depends on the vibrational properties of the lattice by dependence on the phonon frequency distribution $f(\omega)$, and $Q\gamma(0) = 2\lambda_s$ is the Debye-Waller function which describes the time-averaged squared displacement of a molecule in the lattice. Its analytic expression is

$$\lambda_s = \int_{-\infty}^{\infty} p_s(\beta)\, e^{-\beta/2}\, d\beta\,, \tag{23}$$

where

$$p_s(\beta) = \frac{\rho(\beta)}{2\beta\sinh(\beta/2)}\,, \tag{24}$$

with the phonon frequency distribution $\rho(\beta)$. It should be noted that $f(\omega)$ and $\rho(\beta)$ are equivalent. The second exponential can now be treated with the so-called phonon expansion, i.e.

$$\exp(Q[\gamma(t)-\gamma(0)]) = \exp[-Q\gamma(0)]\left[1 + Q\gamma(t) + \frac{Q^2}{2}\gamma^2(t) + ...\right]\,, \tag{25}$$

and then applying a Fourier transformation to every power of $\gamma(t)$; as a result the transform of $\gamma(t)/\gamma(0)$ is

$$g(\omega-\omega_0) = \frac{1}{2\pi}\int_{-\infty}^{\infty} \exp[i(\omega-\omega_0)t]\frac{\gamma(t)}{\gamma(0)}\,dt\,, \tag{26}$$

and thus

$$g(\omega) = \frac{f(\omega)}{\omega(\gamma(0))} \frac{\coth(\beta\omega) - 1}{2} \,. \tag{27}$$

The Fourier transform of every power of $\gamma(t)$ is then

$$G_n(\omega - \omega_0) = \int_{-\infty}^{\infty} g(\omega - \omega_1)\, g(\omega_1 - \omega_2) ... g(\omega_{n-1} - \omega_0)\, d\omega_1 ... d\omega_{n-1} \,, \tag{28}$$

where the connection to the phonon frequency distribution $f(\omega)$ becomes apparent. Finally, this is used to express the differential neutron scattering cross section for inelastic scattering

$$\frac{d^2\sigma}{d\Omega d\omega} = A \frac{k}{k_0}\, e^{-2W} \sum_n \frac{(2W)^n}{n!}\, G_n(\omega - \omega_0) \,. \tag{29}$$

This final equation is related to its scattering kernel by eq. (1) to calculate S_{solid}, however, the overall dynamic structure factor additionally to the solid motion also has a diffusion- or freegas component which is added via a convolution on an α, β-grid [5] and will be discussed in the next section.

2.3.6 Diffusive component

The term *diffusive* component is used here to refer to the part of the self term that is described by either a diffusion equation or by a freegas model. The simpler approximation for the diffusive part of moderator molecules is the freegas, where there is no quantum mechanical interaction between the molecules because the kinetic energy is assumed to be higher than the intermolecular forces. Mathematically, this can be written as [5]

$$S_f(\alpha, \beta) = \frac{1}{\sqrt{4\pi\alpha w_t}} \exp\left(-\frac{(\alpha w_t + \beta)^2}{4\alpha w_t} \right) \,, \tag{30}$$

where w_t is the translational weight which quantifies which ratio of the momentum transfer α goes into the translation of the molecule. The other part w_s goes into internal degrees of freedom described by F. Since moderators are not generally warm enough for the no-interaction condition to hold, diffusion models have been introduced to describe the motion in liquid moderators. There are several possible diffusion models for thermal neutron scattering to choose from, for this thesis the Egelstaff-Schofield model [24] was selected which can be derived by inspecting the the time Fourier-transform of $S_s(\alpha, \beta)$ (index cm being neglected here for brevity):

$$S_s(\alpha, \beta) = \frac{1}{2\pi} \int_{-\infty}^{\infty} I(\alpha, t) \exp(i\beta t) dt \,. \tag{31}$$

In this model, the translational motion is described by the quantity $w(t)$, which is proportional to the mean square displacement of the atom after time t, and is also related to $S_s(\alpha, \beta)$ by:

$$I_s\left(\alpha, t + \frac{i}{2}\right) = \exp[-\alpha w(t)]\,, \tag{32}$$

which graphically describes that displacement within the material will decay over time. It is useful to note, that t does refer to a dimensionless "time" variable. Integrating eq. (31) twice and taking a limit for $\alpha \to 0$, which is a good assumption since the neutrons are considered to be quite low-energy already, yields

$$\lim_{\alpha\to 0}\frac{1}{\alpha}S_s(\alpha,\beta) = \frac{1}{2\pi}\frac{1}{\beta^2}\int_{-\infty}^{\infty}\ddot{w}(t)\exp(i\beta t)\,dt\,, \tag{33}$$

where one can define

$$p_s(\beta) = \beta^2 \lim_{\alpha\to 0}\frac{1}{\alpha}S_s(\alpha,\beta)\,. \tag{34}$$

From eq. (34) it can be seen that $p_s(\beta)$ can be determined experimentally by making neutron scattering experiments with small momentum transfers. By rearranging eq. (33) and integrating the function twice, one can obtain a direct relation between $w(t)$ and $p(\beta)$

$$w(t) = 2\int_0^{\infty}\frac{p_s(\beta)[\cosh\beta/2 - \cos\beta t]}{\beta^2}d\beta\,. \tag{35}$$

Equivalent to the scattering kernel, $w(t)$ may also be separated into a solid and diffusion part

$$w(t) = w_{\text{diff}}(t) + w_{\text{solid}}(t)\,, \tag{36}$$

where the functions $p_{\text{diff}}(\beta)$ and $p_{\text{solid}}(\beta)$ exist as the Fourier-transform of the second derivative of their corresponding $w(t)$. This can thus be related into an equivalent combination of the scattering function S_{diff} and S_{solid} which turns out to be a convolution. The physical motivation for this separation is that a liquid may inherit part of its dynamics from a solid motion and part from a diffusion. However, the main reason for this description is that the computational handling of the problem turns out to be easier. With the relation of $w(t)$ and $S_{\text{diff}}(\alpha, \beta)$ in mind, one can restrict $w_{\text{diff}}(t) \propto 2d|t|$ for large t as well as $w_{\text{diff}}(i/2) = 0$ for small t. The easiest possible expression which allows to accommodate these constraints is

$$w_{\text{diff}}(t) = 2d[(t^2 + c^2 + 0.25)^{1/2} - c]\,. \tag{37}$$

From this, the scattering function for the diffusion contribution is finally

$$S_{\text{diff}}(\alpha,\beta) = \frac{1}{\pi}\exp(2dc\alpha) \cdot \frac{2(c^2+0.25)^{1/2}d\alpha}{[\beta^2+(2d\alpha)^2]^{1/2}} K_1\left((c^2+0.25)^{1/2}[\beta^2+(2d\alpha)^2]^{1/2}\right) . \tag{38}$$

It uses a diffusion coefficient c as well as K_1, the modified Bessel function of the second kind of order 1. It is important to note that the phonon frequency distribution of the translational part includes both a solid and diffusion part. Likewise, the output of a molecular dynamics simulation must be separated by subtracting the diffusion part. The subtracted diffusion term is $p_d(\beta)$ from eq. (34) [24]

$$p_{\text{diff}}(\beta) = \frac{2d}{\pi}(c^2+0.25)^{1/2}\beta\, K_1\left((c^2+0.25)^{1/2}\beta\right) . \tag{39}$$

2.3.7 Combined self part

Following the assumption that the translation can be separated into a solid-type motion and a diffusion motion, the combined self part can then be calculated with a convolution according to the convolution theorem for Fourier transforms. A convolution is a mathematical operation which weighs one function with a second function to produce a third function, which is also called convolution. For this procedure, the second function is reversed and shifted by some value along the integration axis. An integration is performed over the product of the two functions for all (reasonable) values of shift which produces the new function. Specified for this particular problem, one can write for the scattering kernel [5]:

$$S_{s,cm}(\alpha,\beta) = S_t(\alpha,\beta)\, e^{-\alpha\lambda_s} + \int_{-\infty}^{\infty} S_t(\alpha,\beta')\, S_{\text{solid}}(\omega_s\alpha,\beta-\beta')d\beta' , \tag{40}$$

where S_t is either the diffusion model eq. (38) or the freegas model eq. (30) and λ_s is the Debye-Waller coefficient from eq. (23).

2.3.8 Short-collision-time approximation

For large α, the phonon expansion in eq. (25) requires too many terms and the scattering law has to be extended in a different way for higher neutron energy. In NJOY the short-collision-time approximation (SCT) is used for this purpose and NCrystal uses a similar model. When plotting the total cross section with NCrystal one can choose the energy from which the SCT should be used over the standard, convoluted self term. Mathematically, the SCT is related to the freegas model

$$S_s(\alpha,-\beta) = \frac{1}{\sqrt{4\pi w_s\alpha\overline{T}_s/T}} \exp\left(-\frac{(w_s\alpha-\beta)^2}{w_s\alpha\overline{T}_s/T}\right) . \tag{41}$$

The effective temperature is given by

$$\overline{T}_s = \frac{T}{2w_s} \int_{-\infty}^{\infty} \beta^2 \, p_s(\beta) e^{-\beta} \, d\beta \,, \tag{42}$$

with $p(\beta)$ from eq. (24) which depends on the phonon frequency distribution.

3 Water model

3.1 Working with NCrystal

Since NCrystal works with the α, β variables internally and all outputs are also generated this way, from now on every equation and evaluation will only use those parameters. Unrelated to the final goal of a complete scattering model for liquid parahydrogen, the first step undertaken was implementing a water model into the existing NCrystal architecture. As mentioned before, the library can only calculate scattering kernels for polycrystalline materials thus far, which means that liquid water itself cannot be calculated natively. On the other hand, solid water, i.e. ice, can be calculated with a phonon spectrum approach like described in section 2.3.5 using the information about the crystal structure. Using a python interface, this static structure factor can be accessed outside of NCrystal to use it for calculations and then ultimately be fed back into the library to use internal functions to calculate the final cross section. This is then used to check against existing scattering kernels as a benchmark to confirm if the approach works on a simpler material before moving on to the more complex hydrogen implementation.

To obtain the kernel for solid water from NCrystal, one has to provide a file with a phonon spectrum for the given material. The library uses a custom file format called `ncmat` which is a text file that provides information in a way that the library can handle [6]. With the python interface, NCrystal can then create an object called `loadKernel` which calculates the scattering kernel. One has to provide a `vdoslux` parameter which determines the spacing of the energy grid used for the calculation; the highest allowed value being 5. This parameter also determines the size and spacing of the α, β-grid. The grid starts at a small positive value for α, the highest value typically being around 1000. Since neutrons can both, lose and gain energy during interactions with nuclei, the β parameter must have negative values and positive values, although for very cold moderators the scale typically extends further into the negative direction. A useful grid can have size of 50x100 values, but also be much larger, e.g. 400x800.

After using `loadKernel`, the developer can access the necessary information, i.e. the solid-type kernel and the α, β-grid to implement the physics models which is described in the following sections.

3.2 Free gas model

The first model implemented, to allow for easy benchmarking of important core features which are needed later, is the General Atomics (GA) water model [5]. It uses a solid-type motion calculated using phonon expansion convoluted with a free gas model for the translational part, see eq. (30) and eq. (40). In fig. 2 one can see the scattering kernel for the free gas part part alone plotted across the α, β-grid that was used for

this calculation.

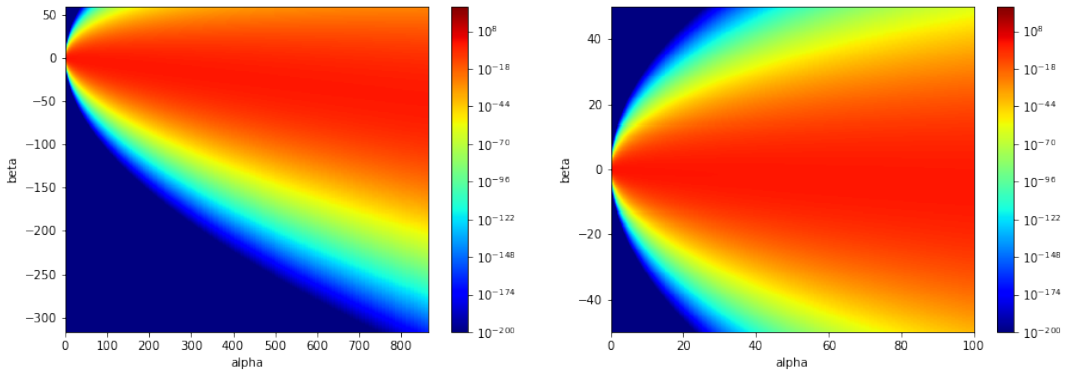

Figure 2: Free gas scattering kernel for eq. (30) used for the GA water model.

In fig. 3, the phonon frequency spectrum used as input to the phonon expansion is plotted. The red dots in the plot show the data points of the phonon frequency spectrum generated with a molecular dynamics simulation. This simulation was not part of the thesis. VDOS means vibrational density of states, i.e. the phonon density at the corresponding energy. These red data points are used as input to the phonon expansion, which yields the solid-type scattering kernel (see section 2.3.5). This process is carried out by NCrystal internally. The blue line is drawn to guide the eye. All plots of the phonon frequency distribution shown in the following sections are to be understood in the same way. In this case, the spectrum also includes the vibrational modes of the dynamic structure factor F, which is visible in terms of the two pronounced peaks at higher energy. This is a third way to include vibrations into the TSL, which is to be differentiated from Young and Koppel who calculated the contribution with operator notation used to compute the matrix elements. Granada et al. used a separate phonon spectrum consisting of δ-functions which was convoluted with the solid-type phonon spectrum. As opposed to cryogenic liquid hydrogen, the water moderator is usually kept around room temperature, thus vibrations may not be neglected. A more thorough theoretical review of neutron scattering in water can be found in the literature, e.g. [3].

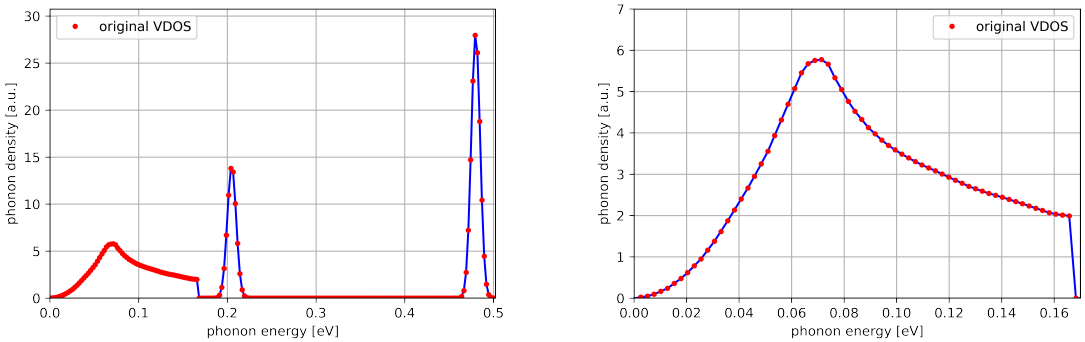

(a) Phonon frequency spectrum used as input for the solid kernel of the GA water model. *Original VDOS* marks the data points used by the phonon expansion. The peaks for higher energy correspond to vibrational modes.

(b) Zoom into the part of the phonon spectrum that is describes the propagation of lattice vibrations.

Figure 3

With this phonon frequency distribution as input, NCrystal is able to calculate the corresponding scattering kernel as discussed in section 2.3.5 and plotted in fig. 4.

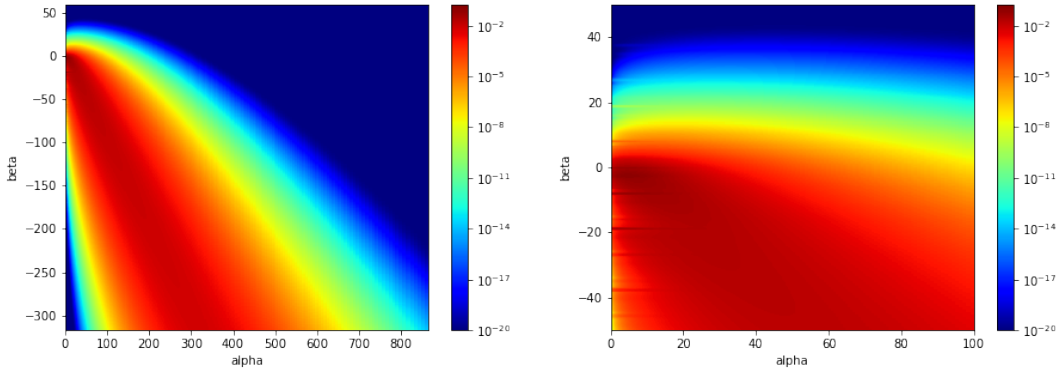

Figure 4: Solid scattering kernel of the GA water model calculated using the phonon frequency distribution from fig. 3.

Regarding the α, β-grid it is important that it represents the shape of the solid kernel as well as the free gas model well enough, such that there is consistent sampling across sharper features. For the free gas there are some sharper features, however, they only occur at the edges for very low momentum transfer and very high downscattering, i.e. a case that is quite unlikely to happen and thus probably does not have an impact on the result. The grid can thus be left unmodified from what NCrystal supplies with vdoslux=4 setting.

From eq. (30) it can be seen that the equation is not evaluated at the position α exactly, but that the parameter is weighted with $\omega_t = 1/18$. For the implementation this does not pose any further problems since there is an analytical expression for the

free gas model which can just be calculated at the weighted α. This changes for the solid contribution which is weighted with $\omega_s = 1 - \omega_t$. Since this scattering kernel is provided by NCrystal and already calculated on a discrete grid, the S_s value at $\omega_s\alpha$ is generally not known. To be able to perform the convolution, the solid kernel thus has to be interpolated in α-direction which makes possible to obtain a functional value for every α within the boundaries of the original grid. The interpolation is done the following way:

$$S_s(\alpha\omega_s) = \frac{S_s[i_2] - S_s[i_1]}{(\alpha[i_2] - \alpha[i_1]) \cdot (\alpha\omega_s - \alpha[i_1])} + S_s[i_1]\,, \tag{43}$$

where $\alpha\omega_s$ is the value that the kernel is interpolated to and evaluated at, i_2 is the index in the α-grid where $\alpha\omega_s$ is sorted into the sequence of increasing values and $i_1 = i_2 - 1$. Graphically this means that $\alpha\omega_s$ is exactly between $\alpha[i_2]$ and $\alpha[i_1]$ and there is a linear interpolation between the two values. For this entire operation, the β-value is fixed since we are only interested in the α-direction. In practical terms it is much faster to do the calculation vectorized for every β simultaneously.

The solid kernel S_s must, however, not only be evaluated at a shifted α but also at a shifted β-position $\beta - \beta'$. As a result, after interpolating in α-direction to find the correct value $S_s(\alpha\omega_s, \beta)$, this shifted grid now has to be interpolated in β-direction as well. This is done using the built-in `scipy` function `interp1d` which can calculate an interpolated function for every $\alpha\omega_s$-row in β-direction at the same time. This function can then be evaluated at any $\beta - \beta'$ value which is necessary for the convolution. In the analytical expression eq. (40) the integration boundaries are set to infinity, but since there is in practice no overlap between the functions at high values, the limit can safely be set at $\beta'_{\text{max}} = \pm 20$. This procedure leads to the final scattering kernel, plotted in fig. 5.

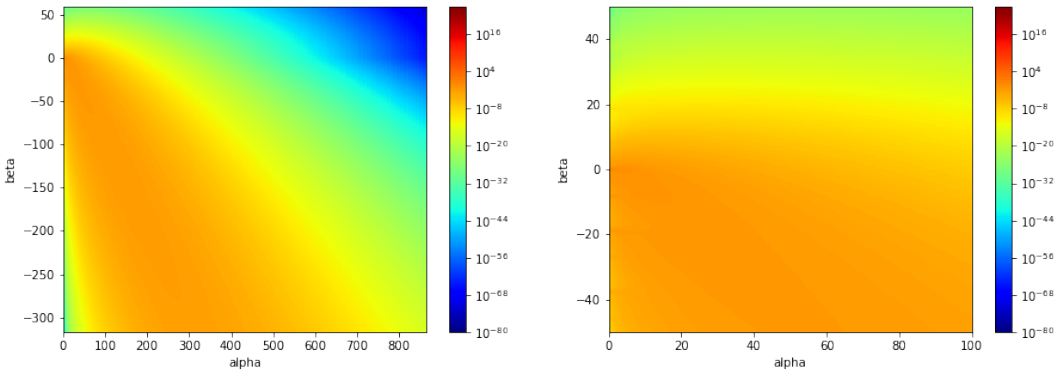

Figure 5: Final scattering kernel as result of the convolution for the GA water model. It combines fig. 2 and fig. 4 according to eq. (40).

The convoluted scattering kernel $S(\alpha, \beta)$ and the grid itself are then written to an `ncmat` file which NCrystal uses to generate the `NCscatter` object. It calculates the

differential cross section according to eq. (1) which, using another NCrystal function, is integrated over all angles to obtain the total neutron scattering cross section σ_n for a given energy range, in this case from 10^{-4} to 10 eV. To see if the convolution and interpolation are correct, the total cross section from the convolution is compared to an earlier GA evaluation in fig. 6.

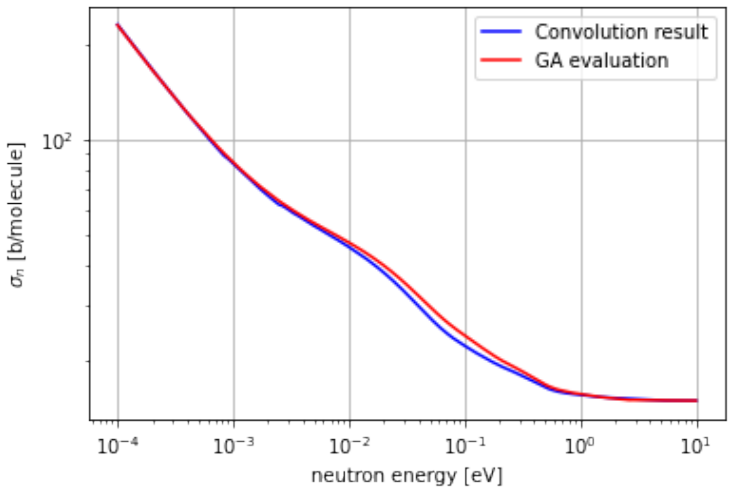

Figure 6: Total neutron scattering cross section of free gas water model at $T = 296$ K compared to GA evaluation [5].

As can be seen in the plot, the agreement with the GA analysis [5] is very good for high and for low energy, some deviations are visible in the intermediate part where the convolution is most important.

3.3 Diffusion model

Water is a liquid at room temperature, which is why the assumption of a free gas for the translational term is not complete. The logical next step is to introduce a model with again a solid-type translation derived from the phonon-frequency spectrum and additionally a diffusion term according to eq. (38). Physically, this means that there is now interaction between between neighboring water molecules (as opposed to the free gas) which in turn influences the neutron cross section. The recoil experienced by a molecule through a scattering event translates into a diffusive motion which depends on momentum and energy transfer. This is different to a purely solid motion where a phonon-only description of the oscillations would suffice. The model investigated here is the CAB model (Centro Atómico Bariloche, Argentina) [25]. It has a different solid term used as input compared to the GA model, i.e. the phonon-frequency distribution is different as can be seen in fig. 7.

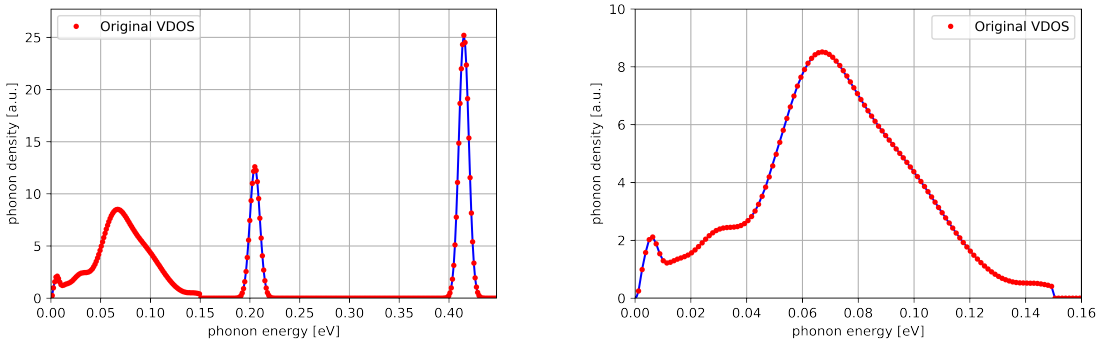

(a) Phonon frequency spectrum used as input for the solid-type contribution of the CAB water model. The peaks for higher energy correspond to vibrational modes. *Original VDOS* marks the data points used by the phonon expansion.

(b) Zoom into the part of the phonon spectrum that is describes the propagation of lattice vibrations. At very low energy, the density is different to the GA model.

Figure 7

Additionally, the diffusion model replaces the free gas and with weights of $w_t = 0.0079$ and $w_s = 1 - w_t$ as well as the diffusion coefficient $c = 3.97$, the diffusion equation eq. (38) yields the kernel in fig. 8.

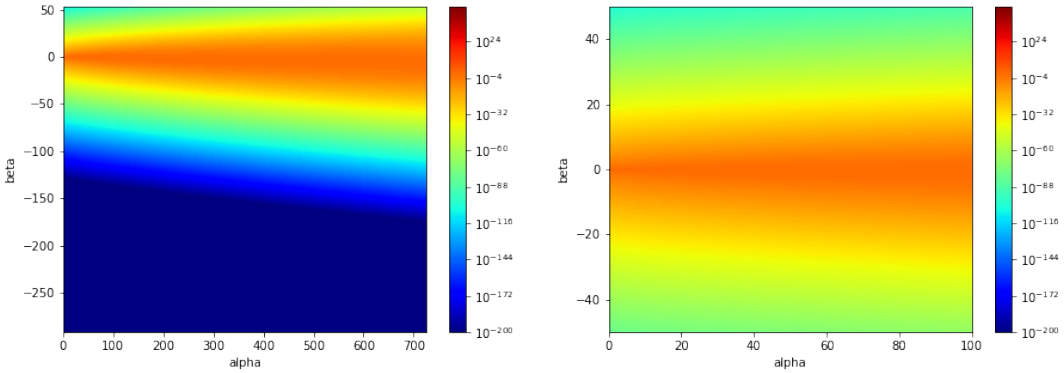

Figure 8: Diffusion scattering kernel for eq. (38) with $w_t = 0.0079$ and $c = 3.97$.

In this case it is useful to show the actual shape of the scattering kernel since it is clearly visible that the contours are relatively sharp along the α-axis, which leads to some computational problems with the α, β-grid. The best way to deal with the problem is to concatenate a logarithmic grid for small β-values with a linear grid for higher values. With the interpolation described in section 3.2, it is no problem to use two different grids - one provided by NCrystal for the solid-type motion and one defined for the diffusion equation.

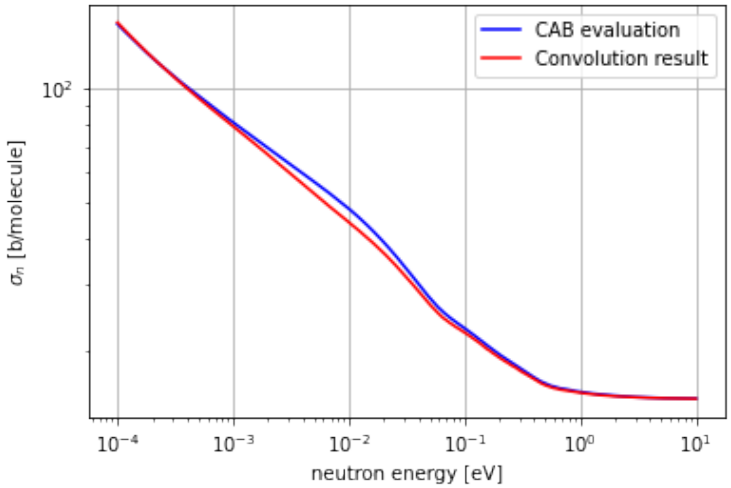

Figure 9: Total neutron scattering cross section of diffusion water model at $T = 293.6$ K compared to CAB evaluation [25].

In fig. 9 the total neutron scattering cross section is plotted for the same energy range as in the free gas case (fig. 6). For comparison, a CAB evaluation of the same model is plotted in the same graph to benchmark the computational accuracy. Generally, the agreement between the two implementations is good which again suggests that the method used is correct. There is a slight deviation for medium energies around 10^{-2} eV. Compared to the free gas model the most striking difference is for low neutron energies where the diffusion model yields values around 40 % lower than the free gas. At the higher end of the energy spectrum both models deliver the same result for the total cross section. A relative comparison between the two models is shown in fig. 10. It makes sense that the largest difference is at low energy since the free gas assumption of no interaction between neighboring molecules breaks down.

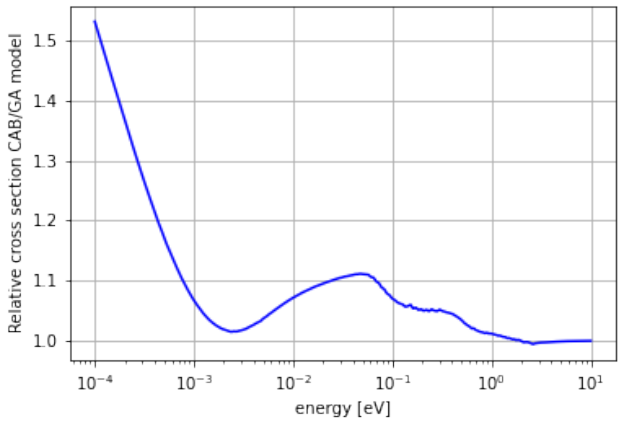

Figure 10: Ratio of the cross section of the two different presented water models. The difference is the most substantial for low neutron energy where the diffusion model's value is 50% lower than that of the free gas model.

4 Hydrogen model

After establishing a working pipeline to interface with NCrystal with the simple water models, the transition to the actual goal of the thesis, liquid hydrogen, is made here.

4.1 Free gas model

The first and simplest model implemented for hydrogen is again the free gas model, described by Young & Koppel [8] as well as in the NJOY manual [5]. Relating it to eq. (5), it drops the distinct $S_{d,cm}$ term as well as all vibrational dependency in the F term, which is valid since the temperature of the liquid hydrogen is 20 K and the molecules thus remain in the lowest vibrational state. In addition to rotational effects, spin correlation between atoms is considered by this model. The NJOY version uses a simple free gas (eq. (30)) for the self part $S_{s,cm}$, without any solid-type motion, which was adapted to this implementation as well. As a result, there is no convolution of different translational parts necessary and the free gas can be directly multiplied into the summation of eq. (5). The resulting scattering kernel for para-hydrogen is plotted in fig. 11.

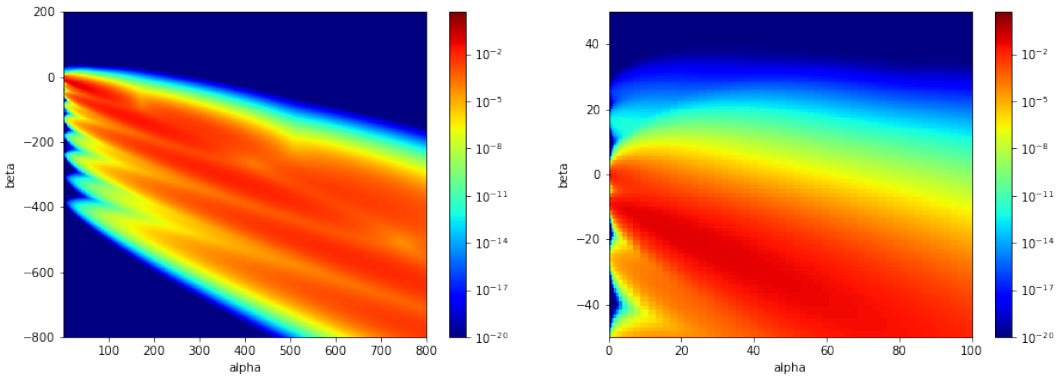

Figure 11: Final scattering kernel for the hydrogen free gas model without any solid-type motion.

The rotational modes are clearly visible as structured energy bands along the β-axis. Since the free gas does neglect any interaction between the molecules, there are no diffusive or coupling effects which blur these bands. To illustrate the rotational modes even more clearly in fig. 12 a cut for one α-value along the β-axis is shown. The bands have been implemented into the model by summation over the respective terms with different J' quantum numbers, as shown in section 2.3.4. In practical terms, the implementation uses six rotational modes, with the contribution of higher J' becoming lower, however, not every rotational mode contributes for every α so it is not surprising that not all modes are visible in a plot like this.

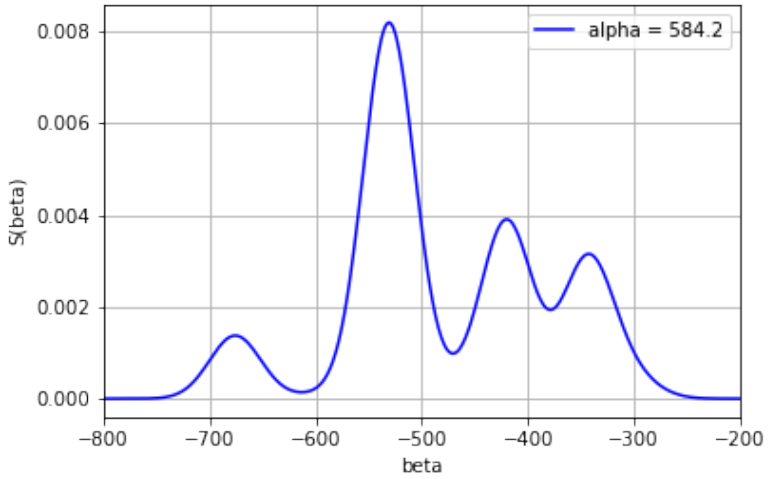

Figure 12: Cut through the scattering kernel along $\alpha = 584.2$ to illustrate the effect of the rotational modes.

In fig. 13a the resulting total cross section for both, ortho- and para-hydrogen is plotted for an energy range from 10^{-4} to 1 eV. For higher neutron energies, both spin correlations of molecular hydrogen have similar cross section. Their characteristic difference at low energies, where para-hydrogen drops to very low values while the cross section of ortho-hydrogen actually increases. The difference arises from the spin-correlation where the parallel nuclear spin alignment of ortho-hydrogen result in the total spin quantum number $S = 1$ and thus, as opposed to para-hydrogen, the odd sums are added. This graph also explains why the ESS requires very pure para-hydrogen as moderator material. Energetic neutrons first encounter the high cross sections on the right side of the graph and are scattered down to lower energies on the left. With ortho-hydrogen, at low energies the cross section increases even more, the neutrons continue to scatter, and cannot escape the moderator, thus becoming unusable for any experiments. Contrast this to para-hydrogen, where the cross section drops significantly at low energies, which allows neutrons that have gotten cold enough as a consequence of many scattering events, to escape the moderator and be guided to the experiments. Graphically, the moderator becomes transparent for low-energy neutrons while it was opaque at higher energy.

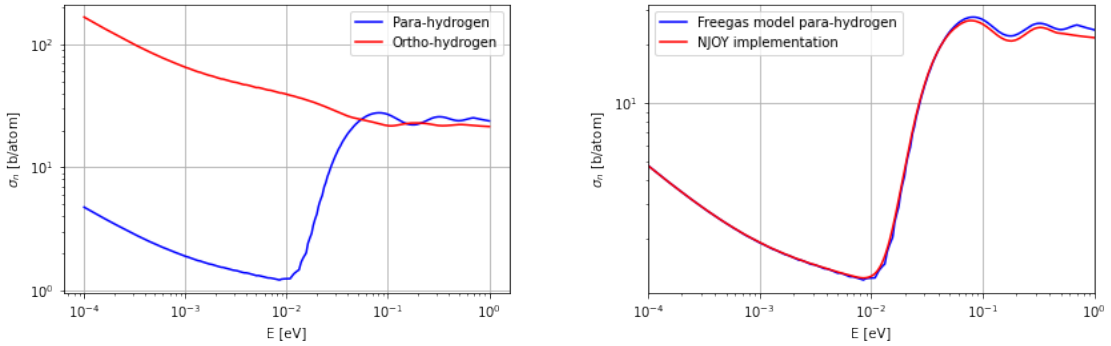

(a) Comparison of ortho- and para-hydrogen total cross sections for the free gas model.

(b) Total cross section of this free gas model implementation compared to the NJOY implementation.

Figure 13

Comparing the calculated cross section of para-hydrogen to the NJOY implementation in fig. 13b, we see very good agreement for low neutron energy and a slight deviation in the thermal range.

4.2 Diffusion model

Since the moderator is cryogenic at $T = 20$ K, the assumption of a free gas for the translational part is not complete. For a better description, a diffusion model based on a convolution of eq. (38) and a solid-type contribution is implemented here. The phonon-frequency distribution used as input for the solid part is plotted in fig. 14 (labeled *original VDOS* in the plot, for thorough explanation see section 3.2). Compared to the water model (fig. 3), it shows a much more pronounced peak at low energies, which indicates a lower resemblance of hydrogen to a solid body compared to water.

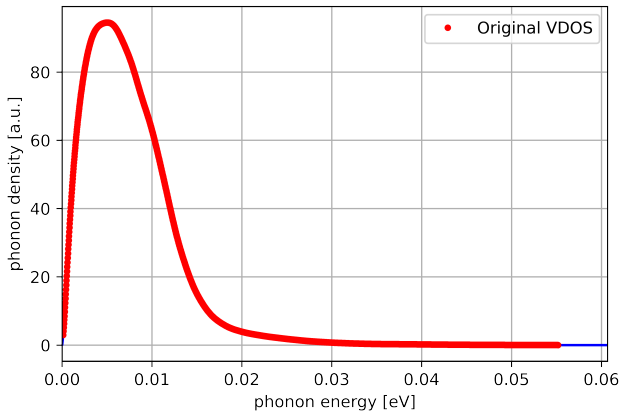

Figure 14: Phonon-frequency spectrum used as input for the solid part of the hydrogen diffusion model. Original VDOS refers to the data points that are used by the phonon expansion. The peak is much more pronounced at very low energies compared to the solid part of the water models.

Compared to the solid kernel of the water models, the hydrogen one looks visually relatively similar, see fig. 15a. Compared to the water model, the weights for solid $w_s = 0.46$ and diffusion part $w_t = 0.040$ are different, as well as the diffusion coefficient with $c = 3.60$. As a result, a stronger contrast can be seen for the diffusion kernel compared to the CAB model. Although there are relatively sharp features visible in fig. 8, it is not as pronounced as in fig. 15b for hydrogen. Considering that the same diffusion model is used, the difference is clearly down to the weights used to compute S_{diff}. For $\alpha \gtrsim 750$ the kernel abruptly drops to 0 which is why values much larger than this have no effect on the convolution result and may thus be neglected to save computing time.

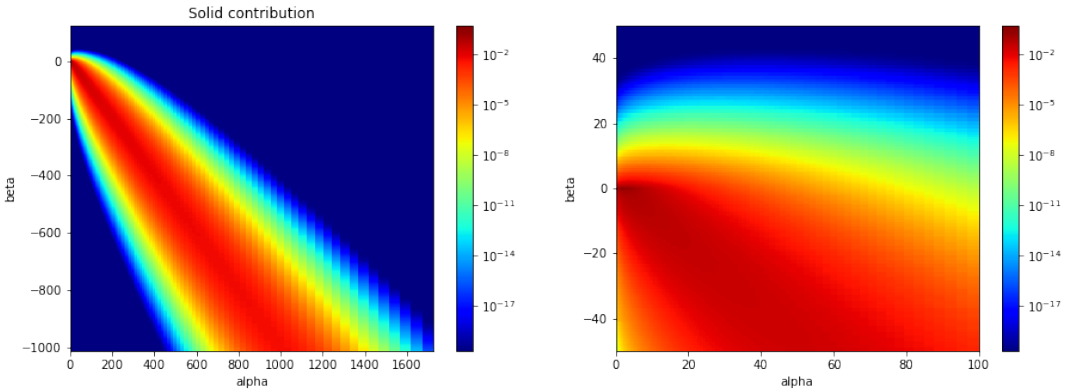

(a) Scattering kernel of the solid part of the diffusion hydrogen model.

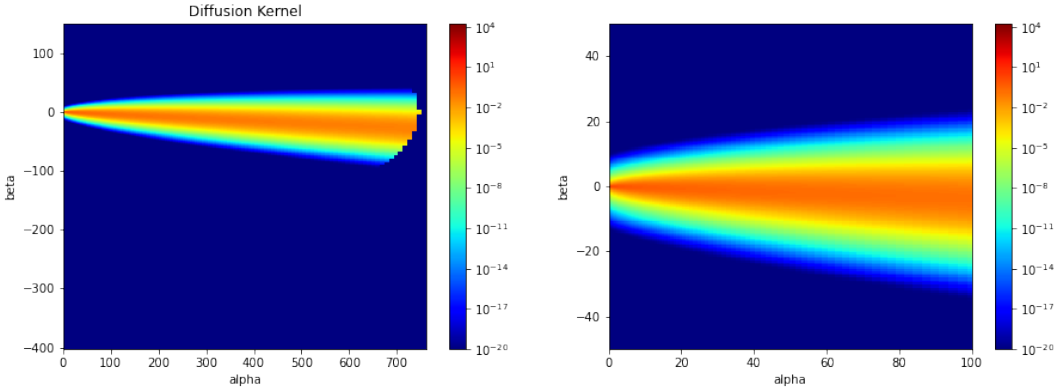

(b) Scattering kernel for the diffusion part of the diffusion hydrogen model.

Figure 15

The convolution of the two parts yields the self part of eq. (5), $S_{s,cm}$. Afterwards, the self part is implemented into the summation over the spin-rotational states, like previously done with the free gas model. However, looking at the free gas case, there was an analytical expression for the self part which could be evaluated at any α, β-position. Since the grid was freely defined before the summation over all the states, the free gas equation could just be multiplied naively in the right place for the right α, β-combination, and the correct result was calculated.

In contrast to that, for the diffusion model, there is no analytical expression of the combined self part after it is generated by the previously described convolution. This is problematic since the self part needs to be evaluated at the position $\beta + \beta_{JJ}$ with

$$\beta_{JJ} = \frac{E'_J - E_J}{k_B T}$$

where $E'_J - E_J$ is the energy difference between two adjacent rotational states. Graphically, this quantity accounts for the fact that some of the energy that would be put into translation of the molecule by a scattering process is actually transformed into a rotational quantum state. To solve this problem, $S_{s,cm}$ is interpolated in β-direction and evaluated at the position $\beta + \beta_{JJ}$, where β_{JJ} needs to be calculated for every combination of the quantum numbers J and J' inside of the summation.

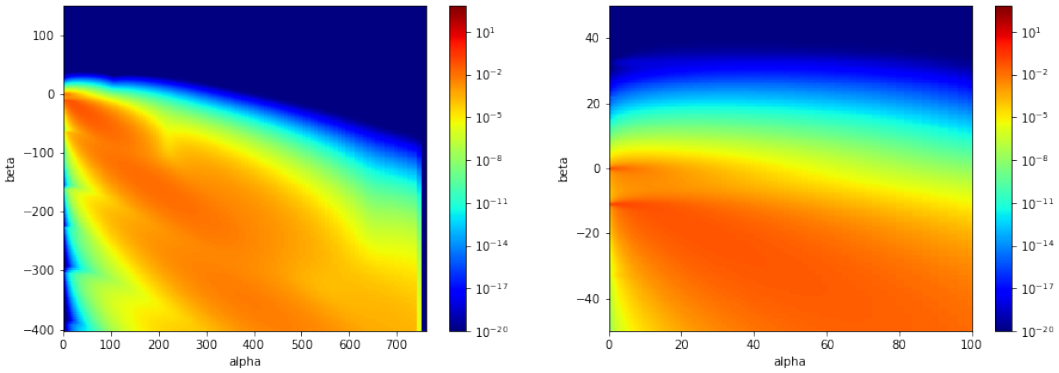

Figure 16: Scattering kernel for para-hydrogen with the diffusion model over the entire α, β-grid.

In fig. 16 the scattering kernel for the diffusion model of para-hydrogen is plotted. The value of the scattering function is a measure of how likely a scattering event of a specific energy transfer β and momentum transfer α is. From this, one can see that there is almost no up-scattering for in this model, i.e. neutrons almost never gain energy when they scatter in liquid para-hydrogen. The ripple-like features on the β-axis also show that the rotational modes of the model are transferred visually into the scattering kernel.

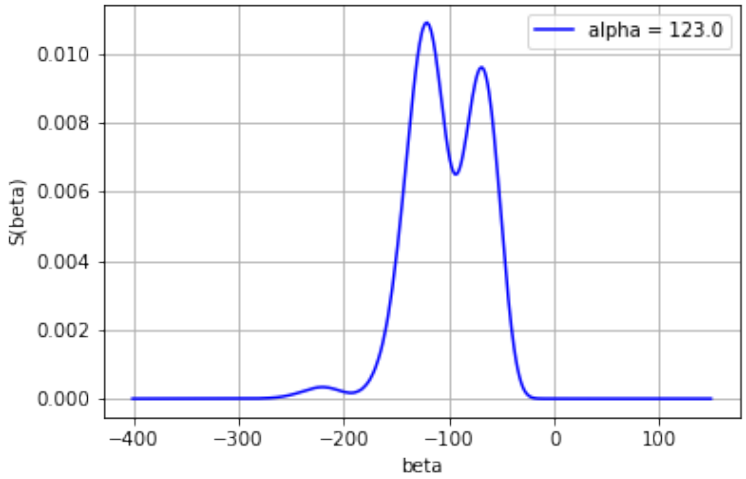

Figure 17: Cut through the scattering kernel at $\alpha = 123$ for all beta values to highlight the features caused by rotational modes.

In fig. 17 the scattering kernel is plotted along $\alpha = 123.0$ for all β-values which highlights three distinct equidistant lines for different energies; essentially a vertical cut through fig. 16. Compared to the equivalent plot for the free gas case in fig. 12 the structure is not quite as pronounced.

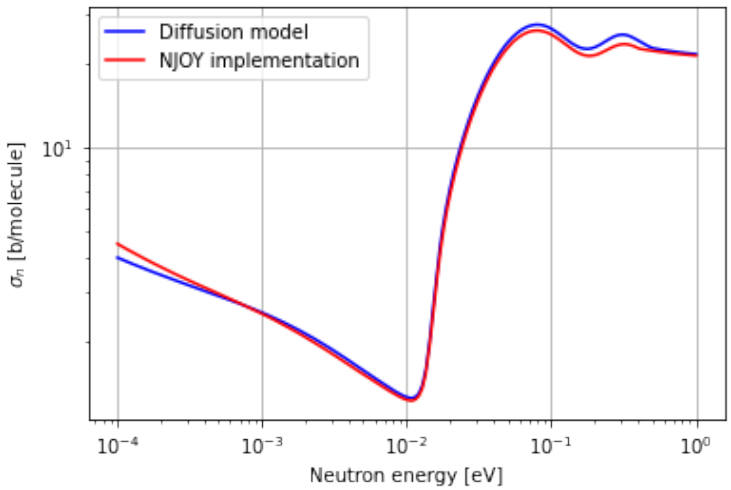

Figure 18: Total neutron scattering cross section of para-hydrogen with the diffusion model (blue) compared the NJOY implementation (red).

In fig. 18 the total cross section for the presented model is plotted compared to the equivalent NJOY implementation. The agreement between the two is generally good, particular during the drop in cross section between 10^{-2} and 10^{-1} eV. At higher energy, one can see the effect of the rotational modes also translate into the cross section. These oscillations are not perfectly matched, however, the result is still satisfactory. At 0.5 eV the diffusion model starts to break down which would be visible by a sharp drop

in cross section for higher energies. To better describe the scattering behavior also in this range, the model is replaced upward of 0.5 eV by a short-collision-time (SCT) approximation (see eq. (41), [5]), which agrees well with NJOY. At low energy, the characteristic of the NJOY model is matched well, with only minor deviations. As will be shown in the next section, the low-energy part is however massively influenced by coherent scattering.

4.3 Coherent scattering model

At low neutron energy, the de Broglie wavelength of neutrons becomes comparable in length to the interatomic distance of hydrogen molecules, hence interference of scattered matter waves is possible, also referred to as coherent scattering. This is what the distinct term $S_{d,cm}$ in eq. (5) refers to which has been neglected thus far. The diffusion model, which is used to calculate the total self part of the scattering kernel, remains the same as before (fig. 15b); according to the aforementioned equation, the coherent part just needs to be added. As a consequence, the phonon frequency distribution remains unchanged as well, see fig. 14. In this case, the Sköld approximation is used to calculate the coherent contribution by using a static structure factor $S(Q)$, see eq. (8). In fig. 19 this factor is plotted against energy. One can see from the plot that for very low neutron wave number the solid part dampens the scattering intensity, and for a neutron wave number above about 5 Å^{-1} there is almost no effect anymore. The highest intensity can be seen at 2 Å^{-1}.

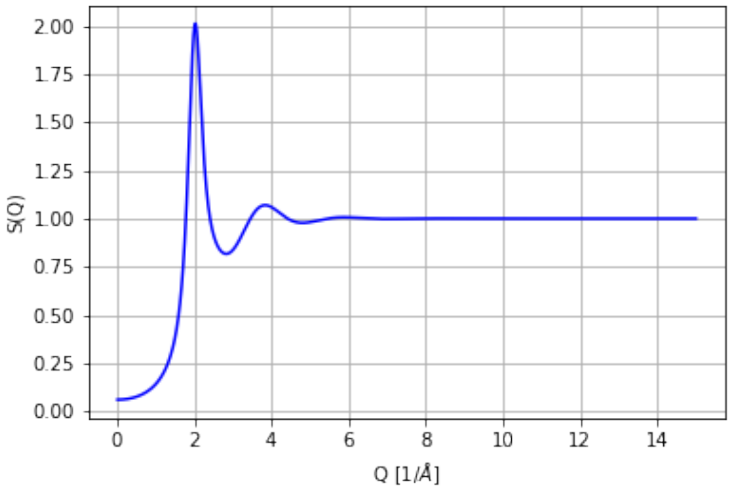

Figure 19: Static structure factor $S(Q)$ used to calculate the coherent scattering contribution.

In practical terms this means that $S(Q)$ has to be evaluated at the wave number of the hydrogen, which is related to its temperature at 15.7 K. To achieve this, $S(Q)$ is interpolated in Q and then evaluated at that exact wave number; this point is called

s_q. As can be seen in eq. (8), the self term $S_{s,cm}$ must then be evaluated at a position $Q' = \frac{Q}{S(Q)}$ which corresponds to the static structure factor which was calculated in the previous step. In α, β-space one can rewrite the argument as $Q' = \frac{\alpha}{s_q}$. Hence, the self term is interpolated in α-direction for every β and then evaluated at Q', which multiplied by s_q is the distinct term. Finally adding the whole self term to the distinct term gives the scattering kernel for coherent scattering in the Sköld approximation which is plotted in fig. 20 for the entire α, β-grid.

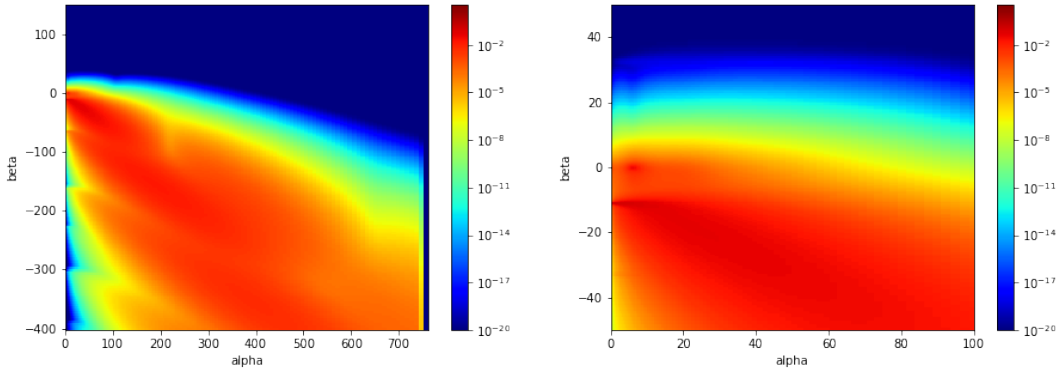

Figure 20: Final scattering kernel for liquid para-hydrogen at $T = 15.7$ K for the Sköld-approximation of coherent scattering.

Generally, the kernel looks quite similar to the one for the diffusion model in fig. 16, again with some obvious features that show the impact of rotational effects on the neutron scattering. To show the difference in the kernel more quantitatively, it was computed in fig. 21 over the entire grid.

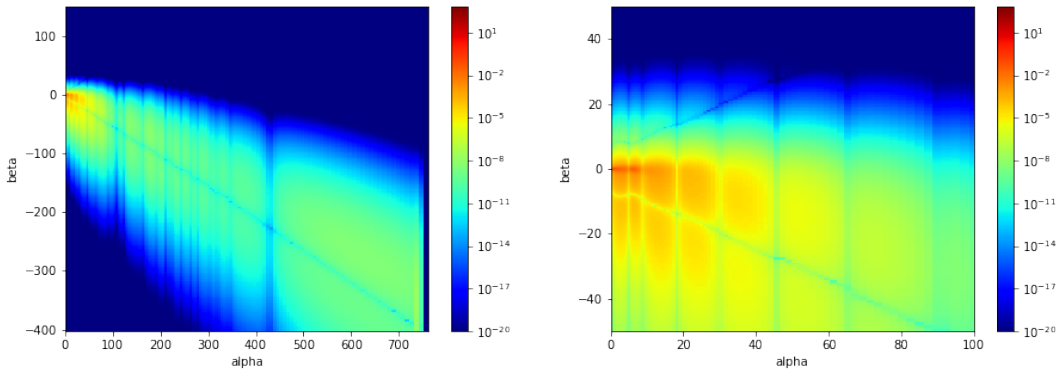

Figure 21: Absolute difference between the scattering kernel of the diffusion model of para-hydrogen and the model which also includes coherent scattering over the entire α, β-grid.

As suggested by the theory, the impact of coherent scattering can mainly be seen at low β, i.e. low neutron energy transfer when the neutron is already close to the equilibrium energy of the moderator and thus bigger changes in energy become more

unlikely. Similar arguments can be made for the concentration of the differences for lower momentum transfer. Some of the sharper features in this plot of differences, like the diagonal edge between $\alpha \approx 20$ to 40 and $\beta \approx 10$ to 30, might also suggest that there are some numerical inaccuracies in the code.

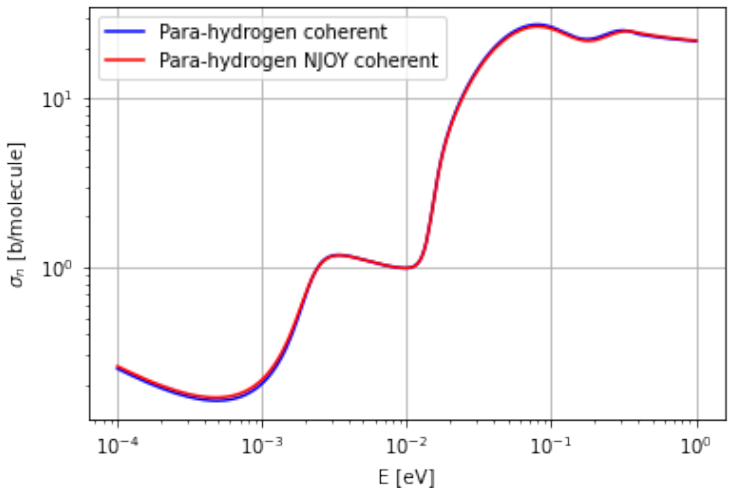

Figure 22: Plot of the total neutron scattering cross section of para-hydrogen at $T = 15.7$ K with coherent scattering implemented into the model.

The total neutron scattering cross section for liquid para-hydrogen at 15.7 K is plotted as the final result in fig. 22. By looking at the difference in the scattering kernel in fig. 21 one could already see that the main difference to the incoherent scattering model is at low energy, which is confirmed here. There is a clear drop in cross section for the coldest neutrons considered for this simulation. This was of course also backed up by the theory earlier in this work.

In terms of the accuracy of the implementation, it is again satisfactory to see very good agreement compared to the NJOY implementation of the model across most of the energy range. There is a very small deviation at very low energy where coherent scattering effects dominate the scattering behavior. It is possible that there is a connection between this and the somewhat nonphysical features which could be seen in the plot of the difference between the incoherent model and this model.

5 Conclusions and Perspective

The objective of this work was to implement a comprehensive model of liquid parahydrogen as a neutron moderator into the NCrystal library. The chosen model, which includes spin-correlation, rotational effects, solid and diffusive translational components, as well as coherent scattering effects at low energy is a complete model of neutron scattering in hydrogen. Benchmarking the final output of this model, the total neutron scattering cross section, against an existing numerical implementation in the leapr module of NJOY shows that the objective has been successfully completed. Confidence in the numerical and physical accuracy of the implementation is increased by the step-wise approach of solving the problem presented in this report. Starting with a simple GA freegas water model, then adding a diffusion component and cross-checking this with existing and much-tested evaluations of water scattering kernels shows, that the fundamental way in which the convolution and interpolation of solid- and diffusion part was done, is accurate. This continues for the implementation of rotation and spin-correlation done for liquid hydrogen, which was also cross checked against existing literature and the previous model from NJOY.

In terms of numerical work, some small deviations in the final cross sections have to be explained, but the developed kernel is good enough to be used in numerical simulations for neutron transport.

Continuous work is necessary on the computational side to implement the python scripts into the NCrystal code base. In terms of additional applications, the now-developed tools can be relatively easily modified to also model neutron scattering in other materials. Related moderators like deuterium or hydrogen-deuteride would be the easiest to implement. Some more changes, also in the physical model, would be necessary to describe methane or other spherical-top molecules which are all materials that are potentially interesting for the application as moderators at neutron sources.

References

[1] Zanini L, Andersen KH, Batkov K, Klinkby EB, Mezei F, Schönfeldt T, et al. Design of the cold and thermal neutron moderators for the European Spallation Source. Nuclear Instruments and Methods in Physics Research, Section A: Accelerators, Spectrometers, Detectors and Associated Equipment. 2019 5;925:33-52.

[2] Garoby R, Vergara A, Danared H, Alonso I, Bargallo E, Cheymol B, et al. The European spallation source design. Physica Scripta. 2018;93.

[3] Bell GI, Glasstone S. Nuclear Reactor Theory. 1st ed. Van Nostrand Reinhold Company; 1970.

[4] Zanini L, Batkov K, Klinkby E, Mezei F, Schönfeldt T, Takibayev A. The neutron moderators for the European Spallation Source. vol. 1021. Institute of Physics Publishing; 2018. .

[5] Macfarlane RE. NEW THERMAL NEUTRON SCATTERING FILES FOR ENDF/B-VI RELEASE 2. 1994 3. Available from: `https://www.osti.gov/biblio/10192168`.

[6] Cai XX, Kittelmann T. NCrystal: A library for thermal neutron transport. Computer Physics Communications. 2020;246:106851. Available from: `http://dx.doi.org/10.17632/s3rpb5d9j3.1`.

[7] Keinert J, Sax J. Investigation of neutron scattering. Kerntechnik. 1987;51.

[8] Young JA, Koppel JU. Slow Neutron Scattering by Molecular Hydrogen and Deuterium*. PHYSICAL REVIEW. 1964;135.

[9] Guarini E. The neutron double differential cross-section of simple molecular fluids: refined computing models and nowadays applications. J Phys: Condens Matter. 2003;15:775-812.

[10] Seiffert WD, Misenta R. Messung der Streuquerschnitte von flüssigem und festem Wasserstoff, Deuterium und Deuteriumhydrid für thermische Neutronen; 1970.

[11] Utsuro M. Slow Neutron Scattering and Intermolecular Excitations in Liquid Hydrogen. Z Physik B. 1977;27:111-6.

[12] Granada JR, Gillette VH, Pepe ME, Sbaffoni MM. Improved thermal neutron scattering kernels for liquid hydrogen and deuterium. Journal of Neutron Research. 2003;11:25-40.

[13] Granada JR, Gillette VH. A new thermal neutron scattering kernel for liquid hydrogen. Physica B: Condensed Matter. 2004 5;348:6-14.

[14] Grammer KB, Alarcon R, Barrón-Palos L, Blyth D, Bowman JD, Calarco J, et al. Measurement of the scattering cross section of slow neutrons on liquid parahydrogen from neutron transmission. Physical Review B - Condensed Matter and Materials Physics. 2015 5;91.

[15] Guarini E, Neumann M, Bafile U, Celli M, Colognesi D, Farhi E, et al. Velocity autocorrelation in liquid parahydrogen by quantum simulations for direct parameter-free computations of neutron cross sections. Physical Review B - Condensed Matter and Materials Physics. 2015 9;92.

[16] Tuckerman ME. Statistical Mechanics: Theory and Molecular Simulation. Oxford University Press; 2010.

[17] Agency NE. International Evaluation Co-operation Volume 42 Thermal Scattering Law S(alpha,beta): Measurement, Evaluation and Application; 2020.

[18] Sköld K. SMALL ENERGY TRANSFER SCATTERING OF COLD NEUTRONS FROM LIQUID ARGON. PHYSICAL REVIEW LETTERS. 1967;19:1023-5.

[19] Damian JIM, Dijulio DD, Muhrer G. Nuclear data development at the European Spallation Source. Journal of Neutron Research. 2021;23:157-66.

[20] Nordin P. Scattering Kernel Calculations for Liquid Para-Hydrogen Using Ring Polymer Molecular Dynamics; 2020.

[21] Huusko A. Calculation of neutron scattering libraries for liquid ortho-deuterium and hydrogen deuteride; 2021.

[22] Guarini E. The neutron cross section of the hydrogen liquids: substantial improvements and perspectives. CRISP. 2014 7;11.

[23] A S. Sjolander - 1958 - MULTI-PHONON PROCESSES IN SLOW NEUTRON SCATTERING. Arkiv för fysik. 1958;14.

[24] Egelstaff PA, Schofield P. On the Evaluation of the Thermal Neutron Scattering Law. Nuclear Science and Engineering. 1962 2;12:260-70.

[25] Damián JIM, Granada JR, Malaspina DC. CAB models for water: A new evaluation of the thermal neutron scattering laws for light and heavy water in ENDF-6 format. Annals of Nuclear Energy. 2014 3;65:280-9.